Capillary pressure and saturation relations for supercritical CO_2 and brine in sand: High-pressure $P_c(S_w)$ controller/meter measurements and capillary scaling predictions

Tetsu K. Tokunaga,[1] Jiamin Wan,[1] Jong-Won Jung,[1,2] Tae Wook Kim,[1,3] Yongman Kim,[1] and Wenming Dong[1]

[1] In geologic carbon sequestration, reliable predictions of CO_2 storage require understanding the capillary behavior of supercritical (sc) CO_2. Given the limited availability of measurements of the capillary pressure (P_c) dependence on water saturation (S_w) with $scCO_2$ as the displacing fluid, simulations of CO_2 sequestration commonly rely on modifying more familiar air/H_2O and oil/H_2O $P_c(S_w)$ relations, adjusted to account for differences in interfacial tensions. In order to test such capillary scaling-based predictions, we developed a high-pressure $P_c(S_w)$ controller/meter, allowing accurate P_c and S_w measurements. Drainage and imbibition processes were measured on quartz sand with $scCO_2$-brine at pressures of 8.5 and 12.0 MPa (45°C), and air-brine at 21°C and 0.1 MPa. Drainage and rewetting at intermediate S_w levels shifted to P_c values that were from 30% to 90% lower than predicted based on interfacial tension changes. Augmenting interfacial tension-based predictions with differences in independently measured contact angles from different sources led to more similar scaled $P_c(S_w)$ relations but still did not converge onto universal drainage and imbibition curves. Equilibrium capillary trapping of the nonwetting phases was determined for P_c ¼ 0 during rewetting. The capillary-trapped volumes for $scCO_2$ were significantly greater than for air. Given that the experiments were all conducted on a system with well-defined pore geometry (homogeneous sand), and that $scCO_2$-brine interfacial tensions are fairly well constrained, we conclude that the observed deviations from scaling predictions resulted from $scCO_2$-induced decreased wettability. Wettability alteration by $scCO_2$ makes predicting hydraulic behavior more challenging than for less reactive fluids.

1. Introduction

[2] Geologic carbon sequestration may become an important technology for mitigating CO_2 buildup in the atmosphere from fossil fuel combustion and for moderating climate change [Intergovernmental Panel on Climate Change (IPCC), 2005]. However, predicting the performance of geologic CO_2 sequestration requires reliable understanding of CO_2 mobility, and its saturation and pressure distribution within reservoirs [Bachu et al., 2007; Bennion and Bachu, 2008; Benson and Cole, 2008]. The dependence of capillary pressure (P_c) on water saturation (S_w) under reservoir conditions is a basic constitutive relation needed to predict CO_2 flow and capillary trapping during sequestration. Indeed, with only knowledge of how (relative) permeability depends on S_w, neither fluid flow nor equilibrium saturation conditions are predictable. At later stages of geologic carbon sequestration, rewetting of reservoirs with native brine results in capillary trapping (residual trapping) of CO_2, a main storage mechanism [Bachu et al., 2007; IPCC, 2005]. The capillary trapping capacity of reservoir materials has complex dependence on porosity, pore-size distribution, nonwetting phase displacement extent, and the rewetting process [Iglauer et al., 2011b; Tanino and Blunt, 2012]. Although capillary trapping of CO_2 at its residual saturation depends on $P_c(S_w)$ relations, few investigations to date have directly measured these basic relations with CO_2/H_2O at reservoir pressures and temperatures [Krevor et al., 2011; Pentland et al., 2011; Pini et al., 2012; Plug and Bruining, 2007]. The study by Plug and Bruining [2007] appears to be the only one in which capillary-trapped $scCO_2$ saturation was determined while

[1]Earth Sciences Division, Lawrence Berkeley National Laboratory, Berkeley, California, USA.
[2]Now at Civil and Environmental Engineering Department, Louisiana State University, Baton Rouge, Louisiana, USA.
[3]Now at Department of Energy Resources Engineering, Stanford University, Stanford, California, USA.

Corresponding author: T. K. Tokunaga, Earth Sciences Division, Lawrence Berkeley National Laboratory, 1 Cyclotron Rd., Berkeley, CA 94720, USA. (tktokunaga@lbl.gov)

controlling P_c as it approached zero during the rewetting process. Given the limited number of experimental measurements of the capillary behavior of CO_2, simulations of CO_2 sequestration in reservoirs commonly rely on modifying more familiar gas (air)/H_2O and oil/H_2O $P_c(S_w)$ relations obtained at atmospheric P and T [*Alkan et al*., 2010; *Doughty*, 2007; *Ide et al*., 2007; *Oldenburg and Doughty*, 2011; *Zhou et al*., 2010], adjusted to account for differences in fluid densities, interfacial tension, and sometimes wettability. However, introduction of supercritical (sc) CO_2 into reservoirs can drive geochemical reactions [*Kaszuba et al*., 2003; *Kharaka et al*., 2006; *Shao et al*., 2011], including wettability alterations [*Bikkina*, 2011; *Chiquet et al*., 2007b; *Dickson et al*., 2006; *Jung and Wan*, 2012; *Y. Kim et al*., 2012]. Thus, its capillary behavior may not be reliably inferred through scaling-based extrapolation of nonreactive immiscible fluids such as air, certain oils, or mercury. The paucity of experimental determinations of $P_c(S_w)$ relations for $scCO_2/H_2O$ is magnified by the fact that reservoir conditions span a very broad range of P, T, and chemistry; over which large variations occur in $scCO_2$ density [*Span and Wagner*, 1996], $scCO_2/H_2O$ interfacial tension [*Bachu and Bennion*, 2009; *Chalbaud et al*., 2010; *Li et al*., 2012], and wettability of mineral surfaces [*Bikkina*, 2011; *Chiquet et al*., 2007a; *Jung and Wan*, 2012; *Wang et al*., 2013].

[3] The present study was conducted in order to better understand the equilibrium capillary behavior of $scCO_2/H_2O$, particularly relative to more familiar air/H_2O capillary relations in uniform sand packs. We first provide an overview of recent experimental studies on the capillary behavior of CO_2 in porous media and then review some basic considerations involved in capillary scaling analyses of $P_c(S_w)$ measurements. This background provides the motivation for the new experiments presented here. Novel aspects of these experiments include measuring repeated drainage and imbibition (rewetting with brine) curves on the same sand pack for air/brine at atmospheric pressure, and $scCO_2$/brine at 8.5 and 12 MPa. This permits testing of capillary scaling predictions through comparisons of these experimental results as well as through scaled comparisons with the many $P_c(S_w)$ relations obtained earlier on uniform sands by other researchers. The two high pressures tested correspond to nominal reservoir depths of 0.8 and 1.2 km and thus are also useful for understanding how $P_c(S_w)$ relations involving CO_2 vary with injection depth. An innovation developed for these experiments is a high-pressure $P_c(S_w)$ controller/meter. As described later, a high-pressure sight glass was used in a configuration such that it simultaneously served three purposes: (1) a $scCO_2$/brine reservoir, (2) a very accurate P_c regulator, and (3) an indicator of volumetric inflow and outflow of brine and $scCO_2$ from the sand. Capillary scaling of the measured drainage and imbibition curves was applied for identifying changes in wettability of the sand over the course of $P_c(S_w)$ experiments.

1.1. Recent Studies of CO_2/H_2O S_w-P_c Relations

[4] Experimental studies on the capillary behavior of $scCO_2/H_2O$ in porous media and comparisons with more familiar fluid/fluid combinations (air/water, oil/water, mercury/air) have become available recently. *Plug and Bruining* [2007] reported drainage and imbibition measurements with distilled water-CO_2(gas), distilled water-CO_2(liquid), and distilled water-$scCO_2$ on quartz sand packs having grain sizes with $360 < D_{50} < 410$ μm. Their experiments with CO_2 in gas and liquid phases conformed to typical drainage and imbibition behavior. However, with $scCO_2$ as the nonwetting phase (8.5 MPa, 40°C), their drainage curve exhibited instabilities in P_c, and their imbibition curves exhibited a shift to lower P_c. The lower magnitude and even negative P_c values were interpreted as indications that the quartz surface became intermediate wettable. Changes in silica surface wettability to varying extents have been reported in other studies conducted under reservoir-relevant $scCO_2$ conditions [*Bikkina*, 2011; *Chiquet et al*., 2007a; *Jung and Wan*, 2012; *Y. Kim et al*., 2012; *McCool and Tripp*, 2005]. *Pentland et al*. [2011] recently presented brine drainage $P_c(S_w)$ relations for brine-$scCO_2$, brine-decane, and air-mercury (Hg injection porosimetry) on Berea sandstone cores and found qualitative agreement among drainage results when capillary-scaled with respect to the Leverett-J function. *Pini et al*. [2012] also measured drainage $P_c(S_w)$ relations for water-$scCO_2$ and air-mercury (Hg injection porosimetry) on Berea and Arqov sandstone cores and obtained much closer agreement among Leverett-scaled $P_c(S_w)$ results. New experimental methods coupling multiphase (CO_2-water) flow with X-ray computed tomography are providing insights into CO_2 trapping associated with finer-scale (subcore, down to $\sim 10^{-3}$ m) heterogeneity [*Perrin and Benson*, 2010; *Pini et al*., 2012]. Even higher-resolution (~14 μm) images obtained with X-ray computed microtomography have yielded images of capillary-trapped $scCO_2$ droplets in reservoir cores [*Iglauer et al*., 2011a]. The emerging understanding of fine-scale controls on CO_2 trapping contributes to making predictions of CO_2 trapping more reliable, given the pore-network-dependent nature of hydraulic properties.

[5] Although the water (brine)-$scCO_2$ behavior in these recent studies for the most part appear to comply with expectations based on capillary scaling, it is important to note that assumptions or adjustments with respect to contact angles and/or interfacial tensions were usually involved. Moreover, most experimental studies have determined only the brine drainage curves, yet hysteresis in $P_c(S_w)$ relations is important for predicting capillary trapping and long-term CO_2 footprint in reservoirs [*Doughty*, 2007; *Iglauer et al*., 2011b; *Juanes et al*., 2010]. Thus, combined drainage and rewetting $P_c(S_w)$ experiments for $scCO_2/H_2O$ under reservoir conditions are needed. Interpretation of results from such experiments may be facilitated through application of capillary scaling analyses.

1.2. Capillary Scaling

[6] Capillary scaling has been used to examine $P_c(S_w)$ relations for immiscible fluids in porous media for many decades [*Haines*, 1930; *Leverett*, 1941; *Miller and Miller*, 1956; *Rose and Bruce*, 1949] and indeed is the foundation for estimating CO_2/H_2O behavior from measurements obtained on air/H_2O and other immiscible fluid systems. Its basis is the Young-Laplace equation:

$$P_c = \frac{2\gamma}{R_m} \tag{1}$$

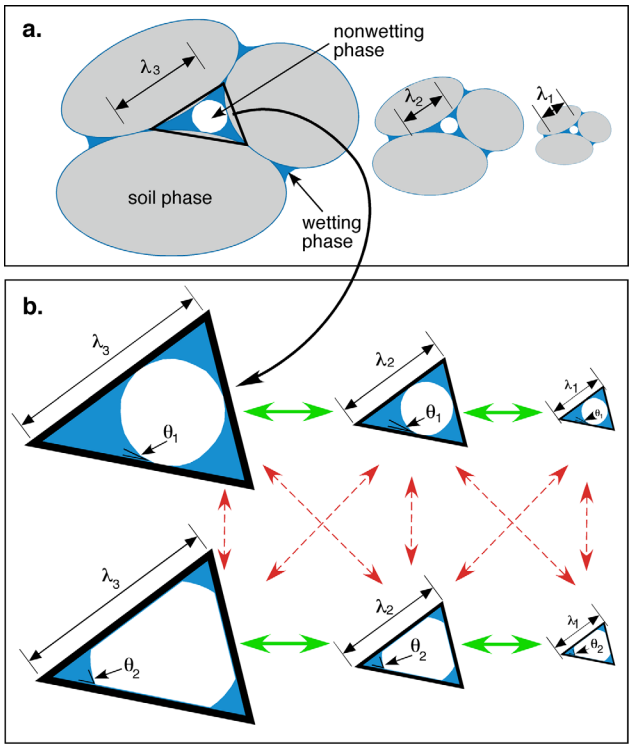

Figure 1. (a) Illustrations of grains in porous media with different characteristic length scales (λ_i). (b) Pore spaces associated with λ_i, with different wetting phase contact angles (θ_i). Transformations consistent with geometric similitude can only occur within systems having a common contact angle (shown by solid green arrows). Changes in wettability result in systems that are not geometrically similar (red dashed lines).

where γ is the fluid-fluid interfacial tension and R_m is the mean interfacial radius of curvature associated with a given P_c. Assigning a capillary length scale λ to either a characteristic pore size or characteristic grain size in a porous medium allows definition of a scaled capillary pressure:

$$\Pi_c = \frac{\lambda P_c}{\gamma} \tag{2}$$

which is predicted to yield a universal drainage $\Pi_c(S_w)$ curve and a separate universal wetting $\Pi_c(S_w)$ curve descriptive of all geometrically similar porous media [*Haines*, 1930; *Klute and Wilkinson*, 1958; *Miller and Miller*, 1956; *Schroth et al*., 1996; *Tokunaga et al*., 2004]. Miller-Miller similitude describes sets of media that are geometrically effectively equivalent in pore network structure when enlarged or reduced in size [*Miller and Miller*, 1956]. Because the porosity n is invariant under such transformations, a set of geometrically similar media has only one n value. When only systems with a common λ are being tested, P_c/γ can be used to as the energy scale [*Parker et al*., 1987; *Plug and Bruining*, 2007], instead of Π_c. As illustrated in Figure 1, geometric similitude further requires that systems all have a common contact angle (not necessarily zero, but constant) in addition to a common value of n [*Miller and Miller*, 1956; *Selker and Schroth*, 1998]. As noted later, strict conformance to the constraint of constant wetting angle is unlikely in the capillary behavior of natural geologic media for several reasons, adding to the challenge of predicting impacts of wetting variations in response to exposure to $scCO_2$.

[7] Experiments on sand columns and dimensional analysis conducted by Leverett led him to propose the scaling relation:

$$J(S_w) = \frac{P_c}{\gamma}\sqrt{\frac{k}{n}} \tag{3}$$

where k is the permeability [*Leverett*, 1941; *Leverett et al*., 1942]. Saturation hysteresis is reflected in separate $J(S_w)$ for water drainage and for water imbibition. The term $(k/n)^{1/2}$ has been regarded as proportional to the porous medium's average pore radius [*Rose and Bruce*, 1949]. Subsequent modifications to the J function have been developed to account for differences in contact angle [*Demond and Roberts*, 1991; *Moseley and Dhir*, 1996; *Rose and Bruce*, 1949], tortuosity [*Garrouch*, 1999], and pore geometry [*Desouky*, 2003], and its application has been extended to consolidated geological media.

[8] Comparing equations (2) and (3) may appear to suggest that λ and $(k/n)^{1/2}$ are directly proportional and interchangeable. Recall however that geometric similitude is restricted to systems having a common value of n. It should also be noted that the n variation in sands used in Leverett's original experiments covered a fairly narrow range (0.38–0.49), thus limiting the range for testing the validity of this scaling approach. Furthermore, in contrast to unconsolidated sands, relations between k, n, and pore-size distributions in consolidated sediments and rocks are considerably less unique [*Bernabe et al*., 2003; *Dullien*, 1992]. Given the wide variation in measured k in cores having approximately similar n, scaling-based generalizations of their unsaturated properties for distinguishing effects of pore structure from those of interfacial and wetting appear very challenging. Measurements on core samples have been very valuable in developing an appreciation for general relations and complexity of $scCO_2$-brine equilibria and flow [*Bennion and Bachu*, 2010; *Krevor et al*., 2011; *Pentland et al*., 2011; *Pini et al*., 2012], but systems with simpler pore geometry offer the opportunity to more easily discern changes in capillary phenomena. Thus, for purposes of evaluating capillary and wetting behavior associated with $scCO_2$ in porous media, measurements of $P_c(S_w)$ relations in a uniform sand have the advantage of being able to make comparisons to an existing large body of experimental characterization with air and oil as the nonaqueous phase [*Klute and Wilkinson*, 1958; *Leverett*, 1941; *Schroth et al*., 1996]. For these reasons, the present study is restricted to comparing $P_c(S_w)$ relations for brine in a single homogeneous sand pack with air and $scCO_2$ as nonaqueous fluid phases.

[9] Given the import effect that wettability has on capillary behavior, a more general scaling of capillary pressure appears possible through including a cos θ term in equation (1), with θ being the contact angle,

$$\frac{\Pi_c}{\cos\theta} = \frac{\lambda P_c}{\gamma\cos\theta} \tag{4}$$

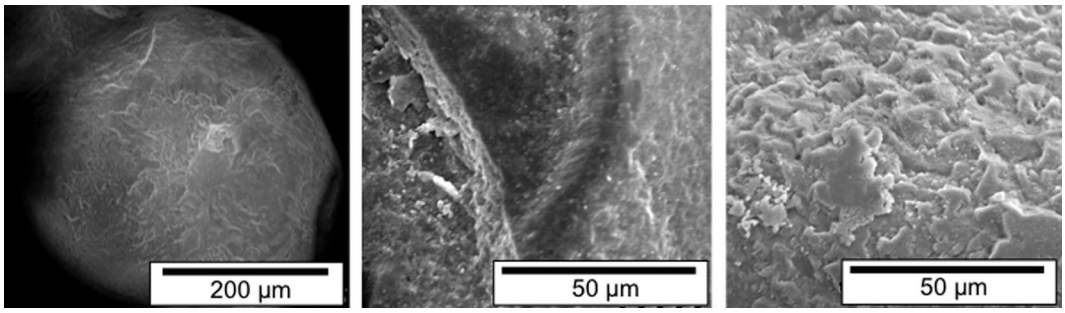

Figure 2. Scanning electron microscope images of quartz sands, showing natural surface roughness and complex microtopography.

[10] Such wettability adjustment is often incorporated in Leverett scaling though a cos θ term included with γ in the denominator. However, unlike contact angle measurements on flat and homogeneous surfaces, wettability in porous media is more complex [*Anderson*, 1986; *Morrow*, 1975]. Receding θ operative during drainage remains very low and fairly insensitive to intrinsic (equilibrium, flat surface) θ, while advancing θ operative during imbibition progressively exceed their intrinsic values above $\theta \approx 45°$ [*Morrow*, 1975]. In addition to complex wetting arising from roughness, porous media are typically comprised of minerals with different wetting properties. Approaches have been developed to incorporate basic wetting properties for modeling capillary behavior in media having mixed or fractional wettability [*Bradford and Leij*, 1996; *O'Carroll et al*., 2006]. Variability of contact angles can also be important during infiltration processes and limit applicability of Miller-Miller scaling of flow [*Selker and Schroth*, 1998]. General inconsistencies arising from including contact angle in scaling have been noted by *Philip* [1969, 1971], although *Parlange* [1974] showed that the limitation is commonly small. Based on these considerations, including a contact angle term in capillary scaling models appears to improve fits only over a moderate range of conditions. In analyses of the experiments described next, scaling with θ will be included to help interpret $P_c(S_w)$ in terms of wettability change.

2. Materials and Methods

2.1. Sand

[11] Moderately well-rounded quartz sand (40–60 mesh, Unimin) was further sieved, and the 250–355 μm size fraction was retained for the experiments. In later scaling analyses, we simply set λ to the midrange grain size of 302 μm. Scanning electron microscope images (Figure 2) show grain surface roughness capable of supporting thick capillary films and facilitating film flow [*Dullien et al*., 1989; *T. W. Kim et al*., 2012; *Or and Tuller*, 2000; *Tokunaga et al*., 2003]. The sand was wet-packed to full saturation at $n = 0.381$ (pore volume 63.4 mL, bulk density 1.64 Mg m^{-3}) within a stainless steel ring (internal diameter 82.1 mm, height $H = 30$ mm), which was placed inside the sample chamber. Permeability measurements with 1 M NaCl obtained on a separate sample of the sand (packed to the same n) yielded a k value of 3.9×10^{-11} m^2 (hydraulic conductivity of 3.9×10^{-4} m s^{-1}).

2.2. Sample Chamber

[12] Our sample chamber design is shown in Figure 3 (used for both atmospheric and high-pressure experiments). A 316 stainless steel porous plate (1 μm pore size, 3.0 mm thick, 94.7 mm diameter, Mott Corp.) is fitted into the bottom cavity of a high-pressure vessel (Parr Instrument Co.). The ring for containing the sand sample is set on top of the stainless steel porous plate, after which the sand was packed as described previously. A hydrophobic C276 Hastelloy porous plate (60 μm pore size, 3.0 mm thick, 94.7 mm diameter, Mott Corp.) is placed on top of the sand pack, and the chamber is capped with the reactor lid. Tightening the reactor lid with the bolts of a split ring assembly seals the chamber (compression of the lid gasket) and ensures that outflow occurs only via the porous stainless steel plate (compression of the bottom O-ring). It should be noted that the Hastelloy plate did not provide measurable capillary resistance to nonwetting phase entry because of its low wettability (observed water contact angles ranged from 90° to 120°). Thus, entry of the nonwetting phase into the sand pack was identifiable because of necessary application of finite capillary pressures.

2.3. Fluids and Wettability

[13] A 1.00 M NaCl solution was used as the aqueous phase in all experiments. The nonaqueous phases tested

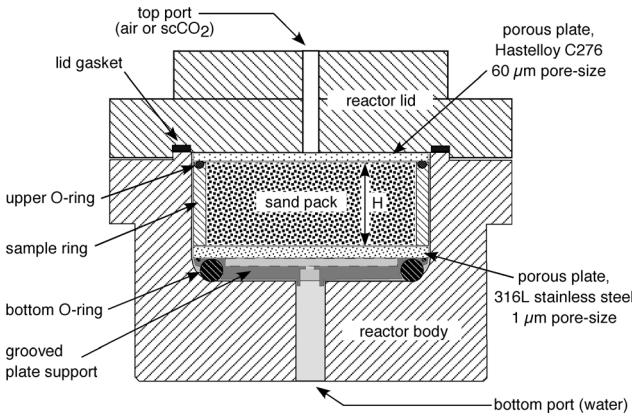

Figure 3. Sample chamber. A high-pressure reaction vessel (Parr Instrument Co.) served as the body of the chamber, with additional components placed in its cavity. The reactor lid is sealed into place with bolts on a pair of split ring clamps (not shown).

Table 1. Fluid-Dependent System Properties Related to Our Experimental Conditions

Temperature	°C	21	45	45
Pressure	MPa	0.102	8.5	12.0
1.00 *M* NaCl density, ρ_w	kg m^{-3}	1036[a]	1032[a]	1034[a]
Nonaqueous phase		Air	$scCO_2$	$scCO_2$
Nonaqueous phase density, ρ_n	kg m^{-3}	1.2	281.8[b]	657.7[b]
$\rho_w - \rho_n$	kg m^{-3}	1035	750	376
$(\rho_w - \rho_n)g$	kg m^{-2} s^{-2}	10,151	7358	3,689
$(\rho_w - \rho_n)gH/2$	Pa	152	110	55
Fluid-fluid interfacial tension, 1.00 *M* NaCl	mN m^{-1}	74.4[c]	33.1 ± 0.5[d]	30.1 ± 0.4[d]
Regression for NaCl/KCl brine [*Li et al*., 2012]			39.1[e]	35.1[e]
75 g/L brine, 8 and 12 MPa [*Bachu and Bennion*, 2009]			32.7[f]	25.5[f]
0.87 *M* NaCl, interpolated *T* [*Chalbaud et al*., 2010]			33[g]	28[g]

[a]The NaCl solution densities were calculated based on the regression equations of *Batzle and Wang* [1992].

[b]Densities of $scCO_2$ were obtained with the NIST web tool, http://webbook.nist.gov/chemistry/fluid/. The $(\rho_w - \rho_n)gH/2$ values represent magnitudes of hydrostatic equilibrium variations in P_c relative to the value at the horizontal midplane of the sample, associated with ± 0.015 m (half the sample height *H*).

[c]Interfacial tension values for 1.00 *M* NaCl-air are from *Weast* [1977].

[d]Interfacial tensions for $scCO_2$-brine were measured in our laboratory using the pendant drop method [*Bachu and Bennion*, 2009].

[e]Estimated interfacial tensions for experiments with $scCO_2$ were obtained by assuming equivalence our NaCl solutions with a solution of monovalent ions comprised primarily of NaCl (86.4%, with 13.6% KCl), and applying the regression relations by *Li et al*. [2012].

[f]Interfacial tensions for a $scCO_2$-brine system with a 75 g/L brine (compared to our 1 *M* NaCl = 68 g/L), at 8 (versus our 8.5) and 12 MPa, 41°C, from *Bachu and Bennion* [2009].

[g]Interpolated values (measurements at 27°C and 71°C) for 0.87 *M* NaCl by *Chalbaud et al*. [2010].

were air at 0.101 MPa, and CO_2 (Airgas, 99.99% purity). As described later, the CO_2 was compressed to its supercritical state, to pressures of 8.5 and 12.0 MPa (45 ± 1 °C), representative of reservoir conditions at about 0.8 and 1.2 km below the land surface. Fluid properties for the experimental conditions are summarized in Table 1. The interfacial tension, γ, clearly is central to capillary phenomena and has only fairly recently been measured in brine-$scCO_2$ systems. Therefore, we conducted our own γ measurements using the pendant drop method [*Bachu and Bennion*, 2009], under the specific conditions relevant for the $P_c(S_w)$ experiments. Our measured values are shown in Table 1. Related γ measurements from the literature obtained under similar conditions to those of our experiments are also included in Table 1 for comparison.

[14] Wettability of the aqueous phase on the silica grain surfaces clearly exerts a critical influence on capillary behavior. We surveyed the recent literature for contact angle measurements obtained under conditions close to those of our experiments. These literature sources consist of experimental measurements [*Bikkina*, 2011; *Broseta et al*., 2012; *Jung and Wan*, 2012; *Y. Kim et al*., 2012; *Mills et al*., 2011; *Wang et al*., 2013], as well as molecular dynamics (MD) simulations [*Iglauer et al*., 2012; *Liu et al*., 2010]. Because few of the systems investigated in the literature involved 1.00 *M* NaCl at our specific experimental conditions, interpolation or extrapolation was usually required. Estimated contact angles relevant for our experimental conditions based on these literature sources are listed in Table 2, along with notes on interpolation or extrapolation used for the listed values. As observed in several of these recent studies [*Iglauer et al*., 2012; *Jung and Wan*, 2012; *Wang et al*., 2013], inconsistencies abound in reported values as well as their trends with respect to changes in salinity, pressure, and temperature.

2.4. $P_c(S_w)$ Measurements at Atmospheric Pressure

[15] The hanging water column method [*Haines*, 1930; *Tokunaga et al*., 2002] was used to obtain brine drainage and imbibition curves under atmospheric pressure. The bottom port of the sample chamber was connected via tubing to the bottom end of a vertically oriented 50 mL pipette. The 8.0 mm ID pipette served as the capillary pressure regulator (through the elevation of the air-water interface

Table 2. Contact Angle Values From Literature Sources, for Experimental Conditions Used in This Study (Brine on Silica, With Air or $scCO_2$)

Temperature (°C)		21	45	45
Pressure (MPa)		0.10	8.5	12.0
Source	Adjustments			
Jung and Wan [2012]	None	35°	52°	56°
Bikkina [2011], 1st cycle	Interpolated *P* and *T*; J&W salinity adjusted[a]		58°	56°
Bikkina [2011], 2nd cycle	Interpolated *P* and *T*; J&W salinity adjusted[a]		85°	79°
Mills et al. [2011]	None; data for 35,000 ppm brine, $P = 12.9$ MPa, $T = 40$°C			27°–32°
Y. Kim et al. [2012]	Middle of measured range (50°–80°)		66°	
Broseta et al. [2012], drain	Interpolated *P* and salinity, $T = 35$°C		35°	35°
Broseta et al. [2012], wet	Interpolated *P* and salinity, $T = 35$°C		60°	65°
Wang et al. [2013]	Interpolated *P* and *T*		20°	21°
Liu et al. [2010]	MD simulations; *P* from CO_2 densities		70°	81°
Iglauer et al. [2012]	MD simulations; interpolated *P* and *T*		70°	73°

[a]Adjusted from 0 to 1 *M* NaCl by increasing the contact angles by about 7° based on *Jung and Wan* [2012].

relative to the elevation of the sample center) as well as a reservoir for measuring outflow/inflow from the sample (labeled in 1 mL increments, volumes interpolated to 0.2 mL). In the atmospheric pressure experiments, the top port of the sample chamber and the upper end of the pipette were simply vented (pin-hole) to the room air (atmospheric pressure). After saturating the sample, the water level in the pipette is adjusted to a position within the bottom portion of the pipette and equilibrated at the horizontal midplane of the sand pack. This configuration allows equilibration to an average $P_c = 0$, with a range within the sand pack of $\pm(\rho_w - \rho_n)gH/2$. In the case of the air-brine system, this variation amounts to ± 152 Pa within the $H = 30$ mm column (Table 1). Drainage curves were obtained by moving the brine-air interface in the pipette successively downward to lower depths, h, relative to the horizontal midplane of the sand pack and recording outflow volumes [*Tokunaga et al.*, 2002]. Equilibrium P_c at each h value was calculated from $(\rho_w - \rho_n)gh$. Imbibition curves were obtained by reversing this procedure through a series of stepwise equilibrations, returning to $P_c = 0$. Time intervals between equilibration steps ranged from 4 h to several days. Two cycles of drainage and rewetting were run with air-brine, after which the $scCO_2$-brine experiments were conducted.

2.5. High-Pressure $P_c(S_w)$ Controller/Meter for $scCO_2$-Brine

[16] The main components for the experimental system were connected via stainless steel tubing and contained within an insulated, T-controlled enclosure maintained at 45°C (±1°C) for the $scCO_2$ experiments (Figure 4). The system's total pressure was controlled with an Isco pump (500D HP, Teledyne, rated to 24 MPa). CO_2 delivered from the pump was preequilibrated with brine in a stirred reactor vessel (Parr 4560 Mini Reactor system, 450 mL, rated to 20 MPa). The high-pressure $P_c(S_w)$ controller/meter simply consisted of a high-pressure sight glass reservoir (Jerguson, 50 mL, rated to 20 MPa) with a volumetric scale superimposed on its window, and its upper and lower ports connected to the sample chamber's $scCO_2$ and brine ports, respectively. The graduated sight glass served the same purpose as the pipette in the atmospheric pressure experiments. The sight glass reservoir was initially placed with its lower window region at the same elevation as that of the upper portion of the sample chamber. The NaCl solution was pumped from the Parr reactor into these components at atmospheric pressure. A rupture disk (20 MPa, Fike Corp.) on the reactor's cap ensured safe venting in case of accidental overpressurization. The initial brine filling of the reservoir and the sample chamber was done at atmospheric P. During this step, the upper purge valve was opened to vent out air and then closed upon emergence of the NaCl solution.

2.6. $scCO_2$-Brine Preparation

[17] The $scCO_2$ and final brine phases were preequilibrated with each other for at least 24 h in the stirred reactor vessel prior to use in experiments. This was accomplished by dispensing liquid CO_2 from the bottom of the gas cylinder via eductor tube into the Isco pump and into the reactor. Brine at atmospheric pressure initially occupied only the sample chamber. The brine-saturated $scCO_2$ was then

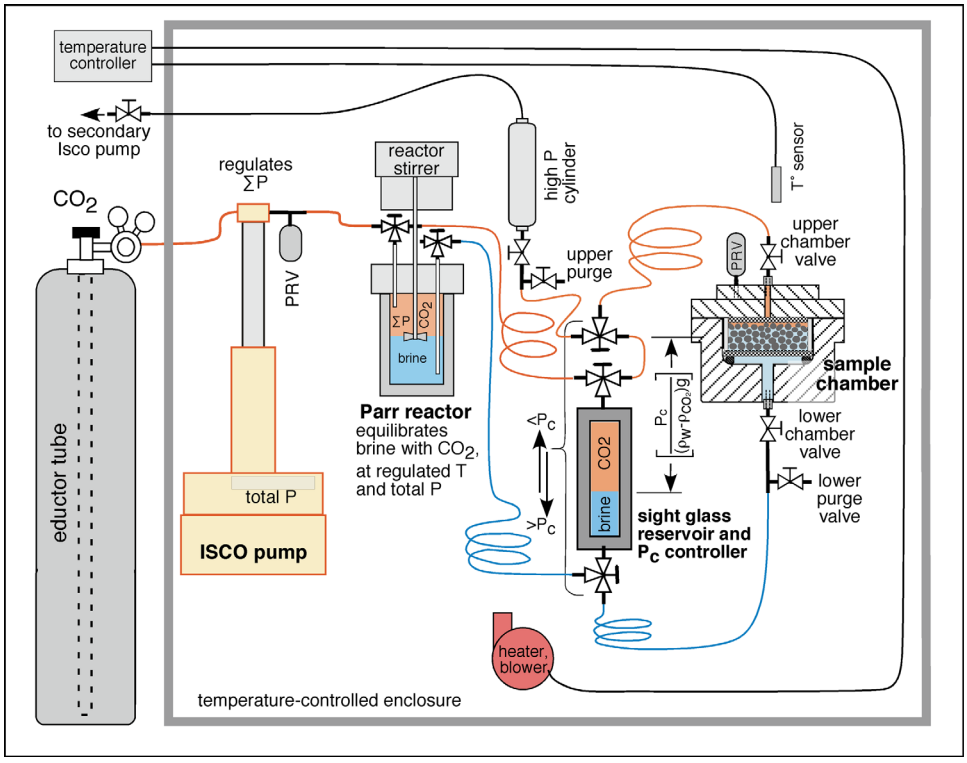

Figure 4. Experimental system. The sample's P_c is controlled by its elevation relative to the $scCO_2$/brine interface in the high-pressure $P_c(S_w)$ controller/meter, which can be moved vertically. Pressure relief valves are located at the pump and on the sample chamber cap.

pumped into the system after closing the lower chamber valve, and further delivery of CO_2 was continued with the Isco pump until the system reached the experimental P (8.5 or 12.0 MPa). Next, the brine saturated with $scCO_2$ was pumped into the high-pressure $P_c(S_w)$ controller/meter and then injected into the sample chamber (in both cases, through their respective bottom ports). During this process, the brine originally in sample chamber (not previously equilibrated with $scCO_2$) was discharged through the upper chamber valve into the high-pressure cylinder (316 stainless steel, 150 mL, 34 MPa rated, Swagelok). The backpressure in the cylinder was maintained at a slightly lower level than the experimental P with a secondary Isco pump. After the sample chamber was purged with at least two pore volumes of $scCO_2$-saturated brine, the upper and lower chamber valves were closed. At this stage, the high-pressure $P_c(S_w)$ controller/meter was repeatedly refilled with brine-saturated $scCO_2$, after which a small amount of $scCO_2$-saturated brine was then introduced in order to bring the brine-$scCO_2$ interface into view at the bottom portion of the window. Next, the cylinder was discharged while isolated from the main system (upper purge valve closed), and the system's total P was controlled at the target value (8.5 or 12.0 MPa) with the main Isco pump. Finally, the vertical position of the high-pressure $P_c(S_w)$ controller/meter was adjusted such that the elevation of the brine-$scCO_2$ interface (in the bottom region of the viewing window) coincided with the center of the sand pack. The upper and lower chamber valves were reopened. In this configuration, the sample chamber and the high-pressure $P_c(S_w)$ controller/meter form a hydraulically closed loop, connected through their respective top valves and bottom valves, and maintained at the experimental total P with the Isco pump.

[18] This closed loop configuration between the sample chamber and the high-pressure $P_c(S_w)$ controller/meter allows control of P_c by setting the level of the $scCO_2$-brine interface in the view window at the desired height h below the sample, as was previously described for the experiments at atmospheric pressure. Therefore, P_c can be controlled to very fine resolution ($\leq$20 Pa), while maintaining the total P at any selected value safely containable by the system [*T. W. Kim et al*., 2012; *Tokunaga and Shuman*, 2010]. Note that this design circumvents the difficulty of regulating P_c using separate P controllers for the two fluid phases. However, because this method relies on adjusting elevations of the reservoir relative to the sample, the practical maximum h is in the range of 1–2 m. Thus, this arrangement is well suited for laboratory experiments designed to simulate $scCO_2$-brine behavior in higher-permeability reservoirs [*T. W. Kim et al*., 2012]. It should be noted again that the P_c values represent conditions at the horizontal midplane of the sand sample, and that variations within the column can be as large as $\pm$110 Pa relative to the midplane value due to the influences of gravity and fluid densities (Table 1). The starting condition for $S(P_c)$ measurements, with the brine-$scCO_2$ interface in the sight glass at the same elevation as the horizontal midplane of the sand pack, corresponds to an average $P_c = 0$ Pa. Adjustment to this initial condition typically takes several steps because the reservoir's brine-$scCO_2$ interface rises in response to brine drainage from the upper tubing and upper chamber cavity ($scCO_2$ filling). The high-pressure $P_c(S_w)$ controller/meter is next moved down manually to set the $scCO_2$-brine interface at a lower elevation (typically by 10 mm or more) to begin equilibration at a new P_c, periodically lowering its elevation if brine drainage from the sample raises the $scCO_2$-brine interface in the sight glass. Similar to the air-brine measurements, from 4 h to several days were allowed for equilibration. Similar step changes are imposed in order to progressively drain brine from the sample, until a practical "residual saturation" is achieved. The procedure is next continued in the reverse direction by manually raising the high-pressure $P_c(S_w)$ controller/meter through a series of steps, until the system is returned to $P_c \leq 0$. Two drainage-rewetting cycles were run at 8.5 MPa, followed by two drainage-rewetting cycles at 12.0 MPa total pressure. It should be noted that full brine saturation was not achieved when $P_c = 0$ was reached during rewetting cycles. In order to obtain higher brine saturations in the sand pack prior to the next drainage run, the brine-$scCO_2$ interface level in the high-pressure $P_c(S_w)$ controller/meter was raised to 1 mm ($\pm$1 mm) above the top surface of the sand (16 mm higher, relative to the horizontal midplane of the sample).

3. Results and Discussion

[19] Although the methods employed for measuring relations between P_c and S_w for air-brine and $scCO_2$-brine involved regulating P_c, such that $S_w(P_c)$ directly reflects experimental procedures, results will be presented with P_c as the dependent variable, in terms of $P_c(S_w)$ and $P_c(V_w/V_b)$, where (V_w/V_b) is the volumetric brine content (volume of brine per bulk sand volume). In order to facilitate direct comparisons of the capillary relations obtained under different combinations of fluids and P-T conditions, all drainage curves will be presented together, and all imbibition curves will be presented together on a separate graph. Following presentation of drainage and imbibition curves in $P_c(S_w)$ form, the same data will be shown in scaled forms; scaling initially only with γ as $\Pi_c(S_w)$, then finally scaled with both γ and $\cos\theta$ as $\Pi_c(S_w)/\cos\theta$. Lastly, we consider the capillary-trapped saturations and volumetric fractions of the nonwetting phase (air, $scCO_2$) obtained in each experiment upon reaching $P_c = 0$ in the rewetting process.

3.1. Measured, Unscaled Relations

[20] Drainage and imbibition curves for each condition exhibited good reproducibility within their duplicate runs (Figure 5). In these and subsequent figures, water contents are presented as saturations (lower x axes) and volumetric water contents (upper x axes). Uncertainties in the sample average P_c and volumetric water contents were all less than 20 Pa and 0.012, respectively (uncertainty in $S_w = 0.03$). Measured values are shown as data points, and the continuous curves are fits to the van Genuchten model:

$$\Theta(P_c) = \Theta_r + (\Theta_s - \Theta_r)\left[\frac{1}{1 + (\alpha P_c)^n}\right]^m \tag{5}$$

where Θ is the volumetric water content (V_w/V_b), Θ_s and Θ_r are the saturation and residual values, respectively, and α (Pa^{-1}), m, and n are fitting parameters [*van Genuchten*, 1980]. Corresponding saturation values S, S_s, and S_r are obtained by dividing volumetric water contents by the

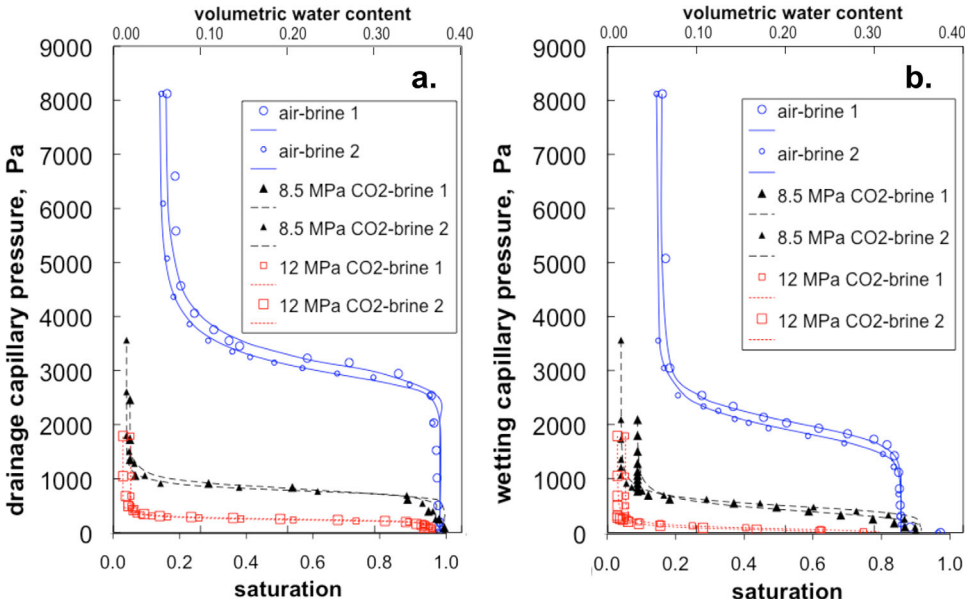

Figure 5. P_c dependence on brine (1 *M* NaCl) phase saturation during (a) drainage and (b) rewetting. Complete saturation is equivalent to a volumetric water content of 0.381. The sequence of experiments involved duplicate drainage-rewetting cycles for air-brine, followed by duplicate cycles with $scCO_2$ at 8.5 MPa, and finally duplicate cycles with $scCO_2$ at 12 MPa.

porosity (0.381). It should be noted that this model was simply applied to provide continuous curves through data to aid in visual comparisons, such that *m* and *n* were varied independently, and Θ_s and Θ_r were usually set to the highest and lowest values obtained for a given run (draining or wetting). The van Genuchten Θ_s for imbibition curves of the air-brine data were fit to the plateau region near zero P_c, because the secondary rise at zero P_c was too abrupt to match. Values of the parameters are listed in Table 3.

[21] Three general trends were observed in the $P_c(S_w)$ results going from air-brine, to 8.5 MPa $scCO_2$-brine, to 12.0 MPa $scCO_2$-brine; (1) shifts to lower P_c values associated with any given S_w value, (2) shifts to lower S_r values, and (3) shifts to lower S_w values associated with rewetting to $P_c = 0$. The lower P_c values at intermediate stages of wetting (Figure 5b) relative to corresponding draining under the same conditions (Figure 5a) reflect the expected hysteresis in moisture characteristic curves. Within each process (draining or wetting), shifts to lower P_c are also qualitatively consistent with decreased interfacial tension (Table 1) in going from air-brine (0.1 MPa) to $scCO_2$-brine (8.5 MPa), to $scCO_2$-brine (12 MPa). It should be noted that the first set of curves at 8.5 MPa (denoted 8.5 MPa CO_2-brine 1) was from two different experiments separated by a system leak, and that the starting Θ_r for the wetting curve was anomalously high, possibly because of incomplete prior drainage.

Table 3. van Genuchten Parameters of Curve Fits (Equation (5)) to Drainage and Rewetting Curves (Figure 5)[a]

		Θ_s	S_s	Θ_r	S_r	α (Pa^{-1})	n	m
Air-1	Drain	0.375	0.98	0.060	0.16	3.44×10^{-4}	23.5	0.269
	Rewet	0.330	0.87	0.060	0.16	4.96×10^{-4}	9.7	0.795
Air-2	Drain	0.375	0.98	0.053	0.14	3.62×10^{-4}	22.0	0.29
	Rewet	0.330	0.87	0.055	0.14	5.41×10^{-4}	9.0	0.74
8.5 MPa CO_2-1	Drain	0.380	1.00	0.019	0.05	1.26×10^{-3}	13.0	0.64
	Rewet	0.353	0.93	0.033	0.09	2.26×10^{-3}	4.3	1.11
8.5 MPa CO_2-2	Drain	0.370	0.97	0.015	0.04	1.33×10^{-3}	17.0	0.55
	Rewet	0.352	0.92	0.015	0.04	2.04×10^{-3}	6.4	0.80
12 MPa CO_2-1	Drain	0.366	0.96	0.020	0.05	4.36×10^{-3}	12.9	0.63
	Rewet	0.310	0.81	0.020	0.05	9.49×10^{-3}	2.4	1.50
12 MPa CO_2-2	Drain	0.357	0.94	0.011	0.03	4.15×10^{-3}	13.6	0.55
	Rewet	0.250	0.66	0.011	0.03	1.55×10^{-2}	2.6	0.87

[a]Note that Θ_s (and S_s) for rewetting was not forced through data at $P_c = 0$ but instead adjusted to minimize root-mean-square deviations to the full rewetting curves.

[22] The second feature emerging from this set of experiments is a general decrease in Θ_r values in going from the atmospheric pressure to high-pressure $scCO_2$ conditions. For the air-brine measurements, Θ_r values were in the range of 0.05–0.06 ($0.14 \leq S_r \leq 0.16$), typical of values reported for wetting liquids in homogeneous sands [*Gittins et al.*, 2010; *Schroth et al.*, 1996]. The greater displacement of the brine and achievement of "residual" saturations as low as 3% indicates that the sand became more hydrophobic through exposure to $scCO_2$.

[23] The third major difference observed between the air and $scCO_2$ measurements concerns the magnitude of capillary trapping of these nonaqueous phases. For rewetting curves, nearly full brine saturation was reached as the P_c was brought back to zero in the air-brine systems; that is, insignificant capillary trapping of air was observed. In contrast, significantly greater amounts of capillary-trapped nonaqueous phase were observed as P_c approached zero for the $scCO_2$-brine (8.5 MPa) and $scCO_2$-brine (12 MPa) experiments. As shown in Figures 5a and 5b and Table 3, Θ_s reached only 0.353 ($S = 92\%$) at $P_c = 0$ for rewetting at 8.5 MPa, and only Θ_s of 0.31 ($S = 81\%$) to 0.25 ($S = 66\%$) at 12.0 MPa. Given the sequence in which these experiments were conducted (0.1, 8.5, and then 12.0 MPa), these trends in imbibition Θ_s indicate that residual trapping capacity for $scCO_2$ increases with pressure (injection

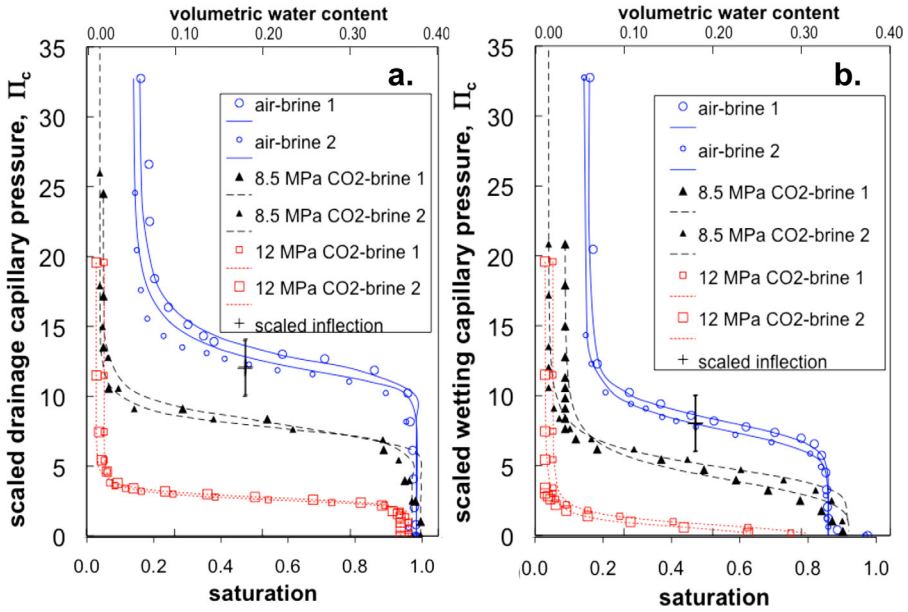

Figure 6. Scaled capillary pressure, $\Pi_c = \lambda P_c/\gamma$, dependence on brine saturation: (a) drainage and (b) wetting curves. Typical values of inflection point Π_c observed in other homogeneous sands are included for comparisons. Values of γ used are from this work and are listed in Table 1.

depth) and/or $scCO_2$ exposure time. The capillary-trapped quantities of $scCO_2$ are considered in greater detail in later discussions.

3.2. Scaling With Interfacial Tension

[24] The extent to which differences in interfacial tension alone can explain differences among the sets of drainage and wetting curves can be evaluated through the scaled capillary pressure $\Pi_c = \lambda P_c/\gamma$. Values of γ for the 1 *M* NaCl-air interface (0.1 MPa, 20°C) and for 1 *M* NaCl-$scCO_2$ interface at 8.5 and 12.0 MPa (45°C) shown in Table 1 are from our own experiments and from literature sources. These values were combined with $\lambda = 302$ μm (middle of the 250 to 355 μm sieve interval) in order to calculate Π_c values. The comparisons of scaled drainage and rewetting curves are presented in Figures 6a and 6b, respectively. Recall that if these systems comply with requirements of geometric (Miller-Miller) similitude, the curves would coalesce onto one unique curve for drainage and another for wetting. From inspection of Figures 6a and 6b, it is evident that accounting for surface tension differences fails to bring the measurements onto single scaled drainage and wetting curves. Therefore, the capillary drainage and wetting behavior of $scCO_2$-brine (1 *M* NaCl) at 8.5 and 12 MPa (45°C) are not predictable when only differences in γ are accounted for. Note that the calculated Π_c relations with S_w for the 12.0 MPa $scCO_2$-brine experiment remain far below those for the scaled air-brine and 8.5 MPa $scCO_2$-brine curves. Thus, additional changes apparently are important in the $scCO_2$-brine systems, especially at the highest pressure, given the relatively small decrease in γ (33.1–30.1 mN m^{-1}) associated with increasing pressure from 8.5 to 12.0 MPa. The possible extent to which changes in wettability could explain lack of universal Π_c relations is considered in section 3.3.

[25] In order to compare our results with a larger database of $P_c(S_w)$ relations, characteristic values for inflection points in scaled drainage and wetting curves have been included in Figures 6a and 6b, respectively. For homogeneous, hydrophilic sands, inflection point Π_c values are approximately 11 and 8, for drainage and wetting curves, respectively [*Tokunaga et al.*, 2004]. Note that scaled air-brine curves agree well with predictions for homogeneous sand. However, at intermediate S_w levels around the drainage and rewetting inflection points, Π_c values obtained with $scCO_2$-brine were shifted from 30% to 90% lower relative to the air-brine reference system. The $scCO_2$-brine curves all fall well below the expected inflection point values, especially at 12.0 MPa.

3.3. Scaling With Interfacial Tension and Contact Angle

[26] In view of the some recent studies on brine-$scCO_2$ contact angles on silica, wettability changes likely caused deviations in $\Pi_c(S)$ relative to results reported in the literature for homogeneous, hydrophilic sands. As previously noted, including the contact angle θ in scaling simply through division of Π_c by cos θ term provides approximate scaling of wettability. This approach was applied to the data in order to examine its predictions. We first consider the θ values listed in Table 2 from the recent study by *Jung and Wan* [2012] on wetting of NaCl brines on smooth silica surfaces under a wide range of CO_2 pressures (up to 25 MPa), and under N_2 at atmospheric P [*Jung and Wan*, 2012]. The θ-scaled drainage and wetting curves are shown in Figures 7a and 7b, respectively. Incorporating θ adjustments in the scaling generally improved matches to the literature-based scaled inflection points for the $scCO_2$-brine systems, although the θ-scaling leads to deviations from the reference inflection points in the air-brine systems. This is expected, given the fact that the earlier studies cited in *Tokunaga et al.* [2004] from which scaled inflection points of 11 (drainage) and 8 (rewetting) were obtained gave no indication that their sands were highly hydrophilic with near-zero

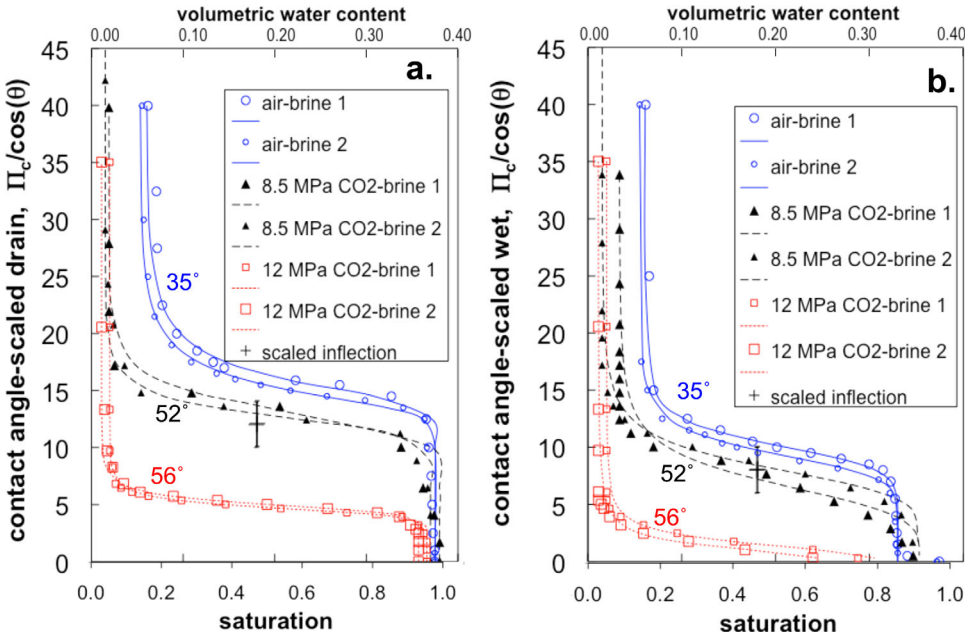

Figure 7. Contact angle-scaled capillary pressure, $\Pi_c/\cos(\theta)$ relations to brine saturation for (a) drainage and (b) rewetting curves. The assigned θ values for brine on smooth silica with air, 8.5 MPa CO_2, and 12 MPa CO_2 are 35°, 52°, and 56°, respectively, as reported by *Jung and Wan* [2012].

θ and lacked mention of pretreatments for enhancing wettability. Moreover, *Selker and Schroth* [1998] showed that the zero contact angle assumption is commonly incorrect. Also recall that *Morrow* [1975] showed that values of drainage θ are effectively 0° for intrinsic θ as large as about 45°. Nonetheless, inspection of Figure 7 leads to the conclusion that the sand pack became less hydrophilic, especially during the final experiments at 12.0 MPa. Even the assumed 56° contact angle was unable to bring the scaled 12.0 MPa curves close to the expected range.

[27] An alternative approach to inferring wettability in these drainage and rewetting curves involves adjusting θ values relative to a reference case assumed to be perfectly hydrophilic. This approach is illustrated in Figure 8, with the air-brine cases assigned $\theta = 0°$. For our experiments with 8.5 MPa CO_2, the $\theta = 52°$ of *Jung and Wan* [2012] was retained based on the satisfactory matching of the inflection point shown previously in Figure 7. The θ-scale drainage and wetting curves at 12 MPa could be fit through the predicted scaled inflection points by assuming $\theta = 77°$

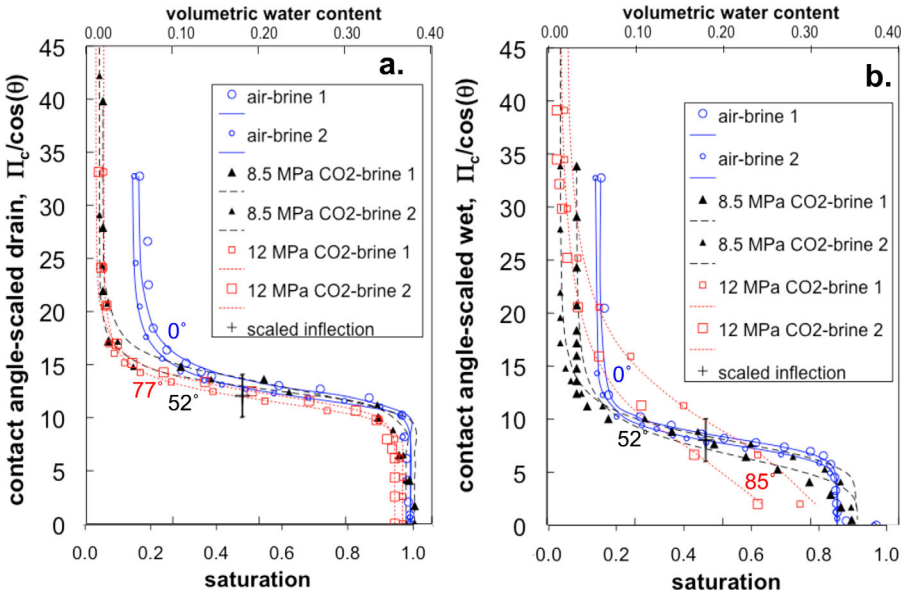

Figure 8. Fitting contact angle-scaled capillary pressure, $\Pi_c/\cos(\theta)$ relations through the scaled inflection points by adjusting the contact angle for (a) drainage and (b) rewetting curves. Assumed contact angles for brine on smooth silica with air, 8.5 MPa CO_2, and 12 MPa CO_2 are 0°, 52°, and 77°/85° (draining/rewetting), respectively.

and 85°, respectively, as shown in Figure 8. Although such adjustments are again inconsistent with geometric scaling, they provide an indication of how much less wettable the sand became through exposure to multiple drainage-rewetting cycles with $scCO_2$.

3.4. Limitations of Capillary Scaling Predictions for $scCO_2$-Brine $P_c(S_w)$

[28] The wide ranges of observed and simulated contact angle values presented in the literature (Table 2) indicate a current lack of consensus on wettabilities of silica surfaces exposed to $scCO_2$ [*Iglauer et al*., 2012]. The study by *Bikkina* [2011] reported significant increases in contact angles (up to 85°) after longer exposure of silica to $scCO_2$. The possibility that fluorine contamination from degradation of polytetrafluoroethylene (PTFE) gaskets in Bikkina's apparatus was proposed as the cause of the observed decreased silica wettability [*Mahadevan*, 2012]. That argument was rebutted by the author [*Bikkina*, 2012], who emphasized the mechanism of $scCO_2$ displacement of adsorbed water [*Dickson et al*., 2006; *Tripp and Combes*, 1998]. Because our sample chamber contained a PTFE gasket, we applied SEM energy dispersive X-ray spectroscopy (SEM-EDS) analyses of quartz sand grain surfaces exposed to $scCO_2$ in our $P_c(S_w)$ experiments, and to control samples (quartz sand grains never exposed to $scCO_2$). These SEM-EDS results yielded no significant differences between the $scCO_2$-exposed versus control samples. Furthermore, lack of X-ray fluorescence peaks at 677 eV (the fluorine K_a energy) in any of the spectra suggests that degradation of our PTFE gasket was not responsible for our observed wettability changes.

[29] Large values of brine-$scCO_2$-silica θ were also recently observed in pores of glass micromodels initially filled with 1 *M* NaCl, shortly after flooding with $scCO_2$ [*Y. Kim et al*., 2012]. The reported θ increases in *Y. Kim et al*. [2012] and *Bikkina* [2011] occurred over much shorter $scCO_2$ exposure times (minutes to days) compared to those of our experiments (months). The other high values of θ (70°–81°) for conditions similar to those of our experiments listed in Table 2 are from MD simulations of wetting [*Iglauer et al*., 2012; *Liu et al*., 2010]. Although these experimental and MD studies suggest that larger θ ($>70°$) values may be characteristic of equilibrium systems, much lower θ ($<25°$) values were obtained in well-equilibrated ($\sim$10 h) measurements of *Wang et al*. [2013].

[30] Hysteresis in advancing versus receding contact angles is another likely reason for some of the poor improvements obtained when scaling with equilibrium θ values obtained from literature sources. Recall that for $\theta > 45°$, *Morrow* [1975] showed that advancing (rewetting) contact angles become greater than their equilibrium values. Contact angle hysteresis could help explain poor prediction of the 12.0 MPa rewetting curves, but not their associated drainage curves.

[31] The collective set of relevant wettability measurements exhibit large variability, with some of these recent studies being qualitatively consistent with changes inferred from our $P_c(S_w)$ measurements on quartz sands exposed to $scCO_2$. Therefore, although θ can be adjusted within the ranges of reported values to fit scaling-predicted relations for $P_c(S_w)$, it is not presently possible to quantitatively predict $P_c(S_w)$ relations between $scCO_2$ and brines. Considerable uncertainties are also associated with relative permeability relations for $scCO_2$-brine in reservoir materials [*Bennion and Bachu*, 2010; *Mathias et al*., 2013]. These studies of $scCO_2$-brine relative permeability behavior along with the $P_c(S_w)$ results presented here underscore the need to conduct more experiments under reservoir conditions in order to gain a better appreciation for probably ranges of capillary behavior. Although it is impractical to perform large numbers of such measurements for each reservoir, better understanding of multiphase equilibrium and flow needs to be developed before reliable long-term predictions can be made.

3.5. Equilibrium Capillary Trapping of $scCO_2$ at $P_c = 0$

[32] Knowledge of the extent to which $scCO_2$ remains trapped within formation pores after cessation of injection and reentry of native brine is important for predicting long-term storage capacities of reservoirs. The hydrodynamics and hydrostatics of capillary trapping of $scCO_2$ are complex, and the experimental challenge of investigating conditions at $P_c \approx 0$ under high pressure can make it difficult to quantify residual saturation of the nonwetting phase. Indeed, our current understanding of $scCO_2$ capillary trapping is largely inferred from experiments conducted at or near atmospheric pressure and room temperature, using other nonwetting fluids such as gas, octane, and mineral oil [*Delclaud*, 1991; *Gittins et al*., 2010; *Iglauer et al*., 2011b; *Pentland et al*., 2008]. Such studies of residual nonwetting phase saturation, S_{nr}, using nonaqueous fluids other than CO_2 yield fairly low values of capillary trapping in homogeneous sand packs, with S_{nr} typically less than 0.13. It should be noted that these S_{nr} are often obtained under somewhat *negative* P_c, i.e., with the aqueous phase at a higher pressure than the nonwetting phase. When $scCO_2$ was used as the nonwetting phase in $P_c(S_w)$ measurements in a sand pack by *Plug and Bruining* [2007], their reported imbibition curve resulted in $S_{nr} \approx 0.5$ at $P_c \approx 0$, and $S_{nr} \approx 0.23$ at $P_c \approx -300$ Pa. Based on this, they concluded that interactions with $scCO_2$ caused a decrease in wettability. Thus, the one previously published measurement of $scCO_2$ S_{nr} in a sand pack indicated that measurements using other nonwetting phase fluids underestimate this quantity for geologic CO_2 sequestration.

[33] Our experimental system and procedure allowed us to examine S_{nr} during the sequence of air-brine, 8.5 MPa $scCO_2$-brine, and 12.0 MPa $scCO_2$-brine imbibition cycles. A closer view of all rewetting curves (previously shown in Figure 5b) in the vicinity of $P_c = 0$ is presented in Figure 9a. The S_{nr} were calculated as $1 - S_w$, at $P_c = 0$, as illustrated by the horizontal arrows in Figure 9a. These trapped nonwetting phase saturations are plotted as a histogram in Figure 9b to facilitate comparisons. Fairly good reproducibility was obtained in the capillary-trapped nonwetting phase volume fractions for air-brine and 8.5 MPa $scCO_2$-brine measurements, and the amounts of $scCO_2$ retained at 12 MPa were distinctly greater. More importantly, the collective results indicate that capillary trapping of $scCO_2$ in silica sands is significantly greater than trapping of air, and that the trapped amounts increase with increased pressure (corresponding to increased reservoir depth). However, because the sequence of air-brine,

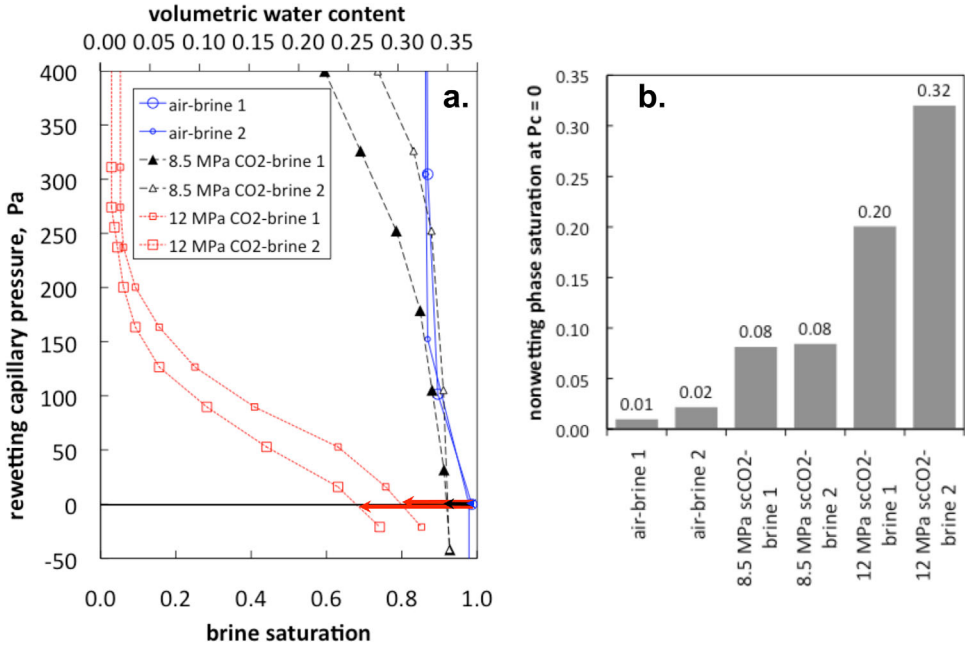

Figure 9. Measured saturations of nonwetting phases obtained upon rewetting to $P_c = 0$. (a) Close-up view of imbibition curves, highlighting departures from rewetting to complete brine saturation (volumetric water content = 0.38). (b) Volumetric fractions of nonwetting phases at $P_c = 0$, shown sequentially over the course of measurements.

8.5 MPa $scCO_2$-brine, and 12.0 MPa $scCO_2$-brine tests also represents the time course of this experiment, effects of $scCO_2$ exposure time may also be important. This possibility is reinforced by the fact that the second test cycle at 12.0 MPa $scCO_2$ resulted in the highest amount of capillary-trapped $scCO_2$ saturation (0.32 versus 0.20 in the first 12.0 MPa cycle). The impact of $scCO_2$ exposure time on its capillary behavior in reservoirs can be quite important, given its anticipated very long residence times and the role of capillary trapping.

[34] Understanding of how residual or capillary trapping of $scCO_2$ depends on wettability properties of reservoirs is just emerging. Studies combining $P_c(S_w)$ and wettability measurements with $scCO_2$-brine still need to be conducted over wider ranges of conditions. Few comprehensive studies of this nature exist, even for oil-water-mineral systems. The systematic measurements of *Jadhunandan and Morrow* [1995] for crude oil-brine in Berea sandstone found that as the wettability was decreased to the intermediate range, residual oil contents decreased. The results from *Jadhunandan and Morrow* [1995] have helped test models for predicting residual oil trapping dependence on wettability [*Spiteri et al.*, 2008; *Valvatne and Blunt*, 2004]. Although it is commonly assumed that capillary trapping of $scCO_2$ can be predicted based on the behavior of oil and gas [*Iglauer et al.*, 2011b; *Pentland et al.*, 2008; *Tanino and Blunt*, 2012], the measurements based on controlled rewetting presented here, and previously by *Plug and Bruining* [2007] indicate otherwise. If $scCO_2$ behaves similarly to the reported and modeled wettability-dependent behavior of oil, less capillary trapping would be observed relative to the reference air-brine system, contrary to our measurements.

[35] Explanations for the discrepancy between measured capillary-trapped $scCO_2$ and expected lower S_{nr} based on oil and gases are beyond the scope of the present study but must result from differences in pore-scale and perhaps interface-scale dynamics of $scCO_2$ versus oil and gas. Based on some previous studies [*Bikkina*, 2011; *Dickson et al.*, 2006; *Tripp and Combes*, 1998], direct interaction of $scCO_2$ with mineral surface can be important, and this could influence contact angle hysteresis, snap-off, and trapping of $scCO_2$ in porous media. Prevention of such direct $scCO_2$-mineral contact by intervening stable aqueous films is expected based on a Derjaguin-Landau-Verwey-Overbeek (DLVO) model [*Tokunaga*, 2012], and $scCO_2$-confined brine films on silica have been measured under controlled P_c [*T. W. Kim et al.*, 2012]. However, the continuum DLVO model does not account for molecular interactions at interfaces, and the measurements of brine films confined by $scCO_2$ were obtained over relatively short times (hours to about 1 day). Evidence that silica surfaces can become $scCO_2$-wet is accumulating [*Bikkina*, 2011; *Dickson et al.*, 2006; *Y. Kim et al.*, 2012; *Plug and Bruining*, 2007; *Tripp and Combes*, 1998], and this may enhance its S_{nr}. Further investigations on the possible increased level of S_{nr} for $scCO_2$ are important to conduct because this will directly affect understanding of reservoir storage capacities.

4. Conclusions

[36] The drainage and wetting $P_c(S_w)$ relations measured in a homogeneous silica sand pack for air-brine and $scCO_2$-brine permitted quantitative comparisons with capillary scaling predictions. These comparisons revealed that the $P_c(S_w)$ relations with $scCO_2$-brine do not comply with expectations from capillary scaling in silica sand, with both brine drainage and rewetting occurring at P_c values of lower than expected magnitudes. Inclusion of contact angle

adjustments in scaling generally improved agreements with predictions, but a fairly wide range of θ are available to choose from, and the theoretical justification for such adjustments for wettability is incomplete. Moreover, P_c values measured for $scCO_2$-brine at 12.0 MPa (45°C) remained well below scaling predictions, even when independently measured contact angles were included. The experimental results also collectively indicate that $scCO_2$ exposure time may be an important factor in altering wettability of silica surfaces. Overall, our results show that $scCO_2$ will enter silica-rich reservoirs more easily than expected because of decreased wettability and will later be stored through capillary trapping at fairly high S_{nr}. More experimental investigations of this type are needed, conducted with $scCO_2$ and different brines, in dominant types of reservoir materials, in order to improve predictions of $scCO_2$ behavior in geologic carbon sequestration. In addition, much longer-term experiments need to be conducted on the stability of capillary-trapped $scCO_2$, given its important contribution in geologic carbon sequestration.

[37] **Acknowledgments.** This work was carried out under funding support from the ZERT, NCGC, and NRAP. The ZERT project was funded by the Assistant Secretary for Fossil Energy, Office of Sequestration, Hydrogen, and Clean Coal Fuels, through the National Energy Technology Laboratory (NETL), U.S. Department of Energy under contract DE-AC02-05CH11231. This material is also based on work supported as part of the Center for Nanoscale Control of Geologic CO_2, an Energy Frontier Research Center funded by the U.S. Department of Energy, Office of Science, Office of Basic Energy Sciences under award DE-AC02-05CH11231. Portions of this work were completed as part of National Risk Assessment Partnership (NRAP) project. Support for this project came from the DOE Office of Fossil Energy's Cross Cutting Research program. The authors wish to acknowledge Robert Romanosky (NETL Strategic Center for Coal) and Regis Conrad (DOE Office of Fossil Energy) for programmatic guidance, direction, and support. NRAP is a multilab effort that leverages broad technical capabilities across the DOE complex. NRAP involves five DOE national laboratories: NETL, Lawrence Berkeley National Laboratory, Lawrence Livermore National Laboratory, Los Alamos National Laboratory, and Pacific Northwest National Laboratory. This team is working together to develop a science-based method for quantifying the likelihood of risks (and associated potential liabilities) for CO_2 storage sites. The work in this paper was reviewed by members of the NRAP Technical Leadership Team, including Jens Birkholzer. NRAP funding was provided to Lawrence Berkeley National Laboratory under U.S. Department of Energy contract DE-AC02-05CH11231. The authors thank Christopher Pentland and the anonymous reviewers for their helpful suggestions that lead to improved presentation.

References

Alkan, H., Y. Cinar, and E. B. Ulker (2010), Impact of capillary pressure, salinity and in situ conditions on CO_2 injection into saline aquifers, *Transp. Porous Media*, *84*, 799–819.

Anderson, W. G. (1986), Wettability literature survey. Part 2: Wettability measurement, *J. Pet. Technol.*, *38*(12), 1246–1262.

Bachu, S., and D. B. Bennion (2009), Interfacial tension between CO_2, freshwater, and brine in the range of pressure from (2 to 27) MPa, temperature from (20 to 125) degrees C, and water salinity from (0 to 334 000) mg L^{-1}, *J. Chem. Eng. Data*, *54*(3), 765–775.

Bachu, S., D. Bonijoly, J. Bradshaw, R. Burruss, S. Holloway, N. P. Christensen, and O. M. Mathiassen (2007), CO_2 storage capacity estimation: Methods and gaps, *Int. J. Greenhouse Gas Control*, *1*, 430–443.

Batzle, M., and Z. Wang (1992), Seismic properties of pore fluids, *Geophysics*, *57*(11), 1396–1408.

Bennion, D. B., and S. Bachu (2008), Drainage and imbibition relative permeability relationships for supercritical CO_2/brine and H2S/brine systems in intergranular sandstone, carbonate, shale, and anhydrite rocks, *SPE Reserv. Eval. Eng.*, *11*(3), 487–496.

Bennion, D. B., and S. Bachu (2010), Drainage and imbibition CO_2/brine relative permeability curves at reservoir conditions for carbonate formations, in *SPE Annual Technical Conference and Exhibition*, p. 18, Soc. of Pet. Eng., Florence, Italy.

Benson, S. M., and D. R. Cole (2008), CO_2 sequestration in deep sedimentary formations, *Elements*, *4*, 325–331.

Bernabe, Y., U. Mok, and B. Evans (2003), Permeability-porosity relationships in rocks subjected to various evolution processes, *Pure Appl. Geophys.*, *160*, 937–960.

Bikkina, P. K. (2011), Contact angle measurements of CO_2-water-quartz/calcite systems in the perspective of carbon sequestration, *Int. J. Greenhouse Gas Control*, *5*, 1259–1271.

Bikkina, P. K. (2012), Reply to the comments on "Contact angle measurements of CO_2-water-quartz/calcite systems in the perspective of carbon sequestration," *Int. J. Greenhouse Gas Control.*, *7*, 263–264.

Bradford, S. A., and F. J. Leij (1996), Predicting two- and three-fluid capillary pressure-saturation relationships of porous media with fractional wettability, *Water Resour. Res.*, *32*(2), 251–259.

Broseta, D., N. Tonnet, and V. Shah (2012), Are rocks still water-wet in the presence of dense CO_2 or H2S?, *Geofluids*, *12*(4), 280–294.

Chalbaud, C., M. Robin, J.-M. Lombard, H. Bertin, and P. Egermann (2010), Brine/CO_2 interfacial properties and effects on CO_2 storage in deep saline aquifers, *Oil Gas Sci. Technol.*, *65*(4), 541–555.

Chiquet, P., D. Broseta, and S. Thibeau (2007a), Wettability alteration of caprock minerals by carbon dioxide, *Geofluids*, *7*(2), 112–122.

Chiquet, P., J. L. Daridon, D. Broseta, and S. Thibeau (2007b), CO_2/water interfacial tensions under pressure and temperature conditions of CO_2 geological storage, *Energy Convers. Manage.*, *48*(3), 736–744.

Delclaud, J. (1991), Laboratory measurement of residual gas saturation, in *Second European Core Analysis Symposium*, pp. 431–451, London.

Demond, A. H., and P. V. Roberts (1991), Effect of interfacial forces on two-phase capillary pressure-saturation relations, *Water Resour. Res.*, *27*(3), 423–437.

Desouky, S. E. D. M. (2003), A new method for normalization of capillary pressure curves, *Oil Gas Sci. Technol.*, *58*(5), 551–556.

Dickson, J. L., G. Gupta, T. S. Horozov, B. P. Binks, and K. P. Johnston (2006), Wetting phenomena at the CO_2/water/glass interface, *Langmuir*, *22*(5), 2161–2170.

Doughty, C. (2007), Modeling geologic storage of carbon dioxide: Comparison of non-hysteretic and hysteretic characteristic curves, *Energy Convers. Manage.*, *48*(6), 1768–1781.

Dullien, F. A. L. (1992), *Porous Media Fluid Transport and Pore Structure*, 2nd ed., 574 pp., Academic, San Diego, Calif.

Dullien, F. A. L., C. Zarcone, I. F. Macdonald, A. Collins, and R. D. E. Bochard (1989), The effects of surface-roughness on the capillary-pressure curves and the heights of capillary rise in glass bead packs, *J. Colloid Interface Sci.*, *127*(2), 362–372.

Garrouch, A. A. (1999), A modified Leverett J-function for the Dune and Yates carbonate fields: A case study, *Energy Fuels*, *13*(5), 1021–1029.

Gittins, P., S. Iglauer, C. H. Pentland, S. Al-Mansoori, S. Al-Sayari, B. Bijeljic, and M. J. Blunt (2010), Nonwetting phase residual saturation in sand packs, *J. Porous Media*, *13*(7), 591–599.

Haines, W. B. (1930), Studies in the physical properties of soil: V. The hysteresis effect in capillary properties, and the modes of moisture distribution associated therewith, *J. Agric. Sci.*, *20*, 97–116.

Ide, S. T., K. Jessen, and F. M. J. Orr (2007), Storage of CO_2 in saline aquifers: Effects of gravity, viscous, and capillary forces on amount and timing of trapping, *Int. J. Greenhouse Gas Control*, *1*, 481–491.

Iglauer, S., A. Paluszny, C. H. Pentland, and M. J. Blunt (2011a), Residual CO_2 imaged with X-ray micro-tomography, *Geophys. Res. Lett.*, *38*, L21403, doi:10.1029/2011GL049680.

Iglauer, S., W. Wulling, C. H. Pentland, S. K. Al-Mansoori, and M. J. Blunt (2011b), Capillary-trapping capacity of sandstones and sandpacks, *SPE J.*, *16*(4), 778–783.

Iglauer, S., M. S. Mathew, and F. Bresme (2012), Molecular dynamics computations of brine-CO_2 interfacial tensions and brine-CO_2-quartz contact angles and their effects on structural and residual trapping mechanisms in carbon geo-sequestration, *J. Colloid Interface Sci.*, *386*, 405–414.

Intergovernmental Panel on Climate Change (IPCC) (2005), Underground geological storage, in *IPCC Special Report on Carbon Dioxide Capture and Storage*, pp. 195–276, Cambridge Univ. Press, Cambridge.

Jadhunandan, P. P., and N. R. Morrow (1995), Effect of wettabiity on waterflood recovery for crude-oil/brine/rock systems, *SPE Reservoir Engineering*, *10*(1), 40–46.

Juanes, R., C. W. MacMinn, and M. L. Szulczewski (2010), The footprint of the CO_2 plume during carbon dioxide storage in saline aquifers:

Storage efficiency for capillary trapping at the basin scale, *Transp. Porous Media*, *82*(1), 19–30.

Jung, J.-W., and J. Wan (2012), Supercritical CO_2 and ionic strength effects on wettability of silica surfaces: Equilibrium contact angle measurements, *Energy Fuels*, *26*, 6053–6059.

Kaszuba, J. P., D. R. Janecky, and M. G. Snow (2003), Carbon dioxide reaction processes in a model brine aquifer at 200 degrees C and 200 bars: Implications for geologic sequestration of carbon, *Appl. Geochem.*, *18*(7), 1065–1080.

Kharaka, Y. K., D. R. Cole, S. D. Hovorka, W. D. Gunter, K. G. Knauss, and B. M. Freifeld (2006), Gas-water-rock interactions in Frio formation following CO_2 injection: Implications for the storage of greenhouse gases in sedimentary basins, *Geology*, *34*(7), 577–580.

Kim, T. W., T. K. Tokunaga, D. B. Shuman, S. R. Sutton, M. Newville, and A. Lanzirotti (2012), Thickness measurements of nanoscale brine films on silica surfaces under geologic CO_2 sequestration conditions using synchrotron X-ray fluorescence, *Water Resour. Res.*, *48*, W09558, doi:10.1029/2012WR012200.

Kim, Y., J. Wan, T. J. Kneafsey, and T. K. Tokunaga (2012), Dewetting of silica surfaces upon reactions with supercritical CO_2 and brine: Pore-scale studies in micromodels, *Environ. Sci. Technol.*, *46*, 4228–4235.

Klute, A., and G. E. Wilkinson (1958), Some tests of the similar media concept of capillary flow: 1. Reduced capillary conductivity and moisture characteristic data, *Soil Sci. Soc. Proc.*, *22*, 278–281.

Krevor, S. C. M., R. Pini, B. X. Li, and S. M. Benson (2011), Capillary heterogeneity trapping of CO_2 in a sandstone rock at reservoir conditions, *Geophys. Res. Lett.*, *38*, L15401, doi:10.1029/2011GL048239.

Leverett, M. C. (1941), Capillary behavior in porous solids, *Trans. Am. Inst. Min. Metal. Eng.*, *142*, 152–169.

Leverett, M. C., W. B. Lewis, and M. E. True (1942), Dimensional-model studies of oil-field behavior, *Trans. Am. Inst. Min. Metal. Eng.*, *146*, 175–193.

Li, X., E. Boek, G. C. Maitland, and J. P. M. Trusler (2012), Interfacial tension of (brines + CO_2): (0.864 NaCl + 0.136 KCl) at temperatures between (298 and 448) K, pressures between (2 and 50) MPa, and total molalities of (1 to 5) mol · kg^{-1}, *J. Chem. Eng. Data*, *57*(4), 1078–1088.

Liu, S. Y., X. N. Yang, and Y. Qin (2010), Molecular dynamics simulation of wetting behavior at CO_2/water/solid interfaces, *Chin. Sci. Bull.*, *55*(21), 2252–2257.

Mahadevan, J. (2012), Comments on the paper titled ''Contact angle measurements of CO_2-water-quartz/calcite systems in the perspective of carbon sequestration'': A case of contamination?, *Int. J. Greenhouse Gas Control, 7*, 261–262.

Mathias, S. A., J. G. Gluyas, G. J. Gonzalez Martinez de Miguel, S. L. Bryant, and D. Wilson (2013), On relative permeability data uncertainty and CO_2 injectivity estimation for brine aquifers, *Int. J. Greenhouse Gas Control*, *12*, 200–212.

McCool, B., and C. P. Tripp (2005), Inaccessible hydroxyl groups on silica are accessible in supercritical CO_2, *J. Phys. Chem. B*, *109*(18), 8914–8919.

Miller, E. E., and R. D. Miller (1956), Physical theory for capillary flow phenomena, *J. Appl. Phys.*, *4*, 324–332.

Mills, J., M. Riazi, and M. Sohrabi (2011), Wettability of common rock-forming minerals in a CO_2-brine system at reservoir conditions, in *Society of Core Analysts*, p. 12, Soc. of Core Anal., Austin, Tex.

Morrow, N. R. (1975), The effects of surface roughness on contact angle with special reference to petroleum recovery, *J. Can. Pet. Technol.*, *14*(4), 42–53.

Moseley, W. A., and V. K. Dhir (1996), Capillary pressure-saturation relations in porous media including the effect of wettability, *J. Hydrol.*, *178*, 33–53.

O'Carroll, D. M., L. M. Abriola, C. A. Polityka, S. A. Bradford, and A. H. Demond (2006), Prediction of two-phase capillary pressure-saturation relationships in fractional wettability systems, *J. Contam. Hydrol.*, *77*, 247–270.

Oldenburg, C. M., and C. Doughty (2011), Injection, flow, and mixing of CO_2 in porous media with residual gas, *Transp. Porous Media*, *90*, 201–218.

Or, D., and M. Tuller (2000), Flow in unsaturated fractured porous media: Hydraulic conductivity of rough surfaces, *Water Resour. Res.*, *36*(5), 1165–1177.

Parker, J. C., R. J. Lenhard, and T. Kuppusamy (1987), A parametric model for constitutive properties governing multiphase flow in porous media, *Water Resour. Res.*, *23*(4), 618–624.

Parlange, J.-Y. (1974), Scaling by contact angle, *Soil Sci. Soc. Am. Proc.*, *38*, 161–162.

Pentland, C. H., S. Al-Mansoori, S. Iglauer, B. Bijeljic, and M. J. Blunt (2008), Measurement of non-wetting phase trapping in sand packs, in *SPE Annual Technical Conference and Exhibition*, p. 11, SPE, Denver, Colo.

Pentland, C. H., R. El-Maghraby, S. Iglauer, and M. J. Blunt (2011), Measurements of the capillary trapping of supercritical carbon dioxide in Berea sandstone, *Geophys. Res. Lett.*, *38*, L06401, doi:10.1029/2011GL046683.

Perrin, J. C., and S. M. Benson (2010), An experimental study on the influence of sub-core scale heterogeneities on CO_2 distribution in reservoir rocks, *Transp. Porous Media*, *82*, 93–109.

Philip, J. R. (1969), *Theory of Infiltration*, edited by V. T. Chow, pp. 215–296, Academic, New York.

Philip, J. R. (1971), Limitations on scaling by contact angle, *Soil Sci. Soc. Am. Proc.*, *35*, 507–509.

Pini, R., S. C. M. Krevor, and S. M. Benson (2012), Capillary pressure and heterogeneity for the CO_2/water system in sandstone rocks at reservoir conditions, *Adv. Water Resour.*, *38*, 48–59.

Plug, W. J., and J. Bruining (2007), Capillary pressure for the sand-CO_2-water system under various pressure conditions. Application to CO_2 sequestration, *Adv. Water Resour.*, *30*(11), 2339–2353.

Rose, W., and W. A. Bruce (1949), Evaluation of capillary character in petroleum reservoir rock, *Trans. Am. Inst. Min. Metal. Eng.*, *186*(5), 127–142.

Schroth, M. H., S. J. Ahearn, J. S. Selker, and J. D. Istok (1996), Characterization of Miller-similar silica sands for laboratory hydrologic studies, *Soil Sci. Soc. Am. J.*, *60*, 1331–1339.

Selker, J. S., and M. H. Schroth (1998), Evaluation of hydrodynamic scaling in porous media using finger dimensions, *Water Resour. Res.*, *34*(8), 1935–1940, doi:10.1029/98WR00625.

Shao, H., J. R. Ray, and Y. S. Jun (2011), Effects of salinity and the extent of water on supercritical CO_2-induced phlogopite dissolution and secondary mineral formation, *Environ. Sci. Technol.*, *45*(4), 1737–1743.

Span, R., and W. Wagner (1996), A new equation of state for carbon dioxide covering the fluid region from the triple-point temperature to 1100 K at pressures up to 800 MPa, *J. Phys. Chem. Ref. Data*, *25*(6), 1509–1596.

Spiteri, E. J., R. Juanes, M. J. Blunt, and F. M. J. Orr (2008), A new model of trapping and relative permeability hysteresis for all wettability characteristics, *SPE J.*, *13*(3), 277–288.

Tanino, Y., and M. J. Blunt (2012), Capillary trapping in sandstones and carbonates: Dependence of pore structure, *Water Resour. Res.*, *48*, W08525, doi:10.1029/2011WR011712.

Tokunaga, T. K. (2012), DLVO-based estimates of adsorbed water film thicknesses in geologic CO_2 reservoirs, *Langmuir*, *28*(21), 8001–8009.

Tokunaga, T. K., and D. B. Shuman (2010), *A Method to Control Low Capillary Pressure Differences Over Arbitrarily High Total Pressures*, Lawrence Berkeley Natl. Lab., Berkeley, Calif.

Tokunaga, T. K., J. Wan, and K. R. Olson (2002), Saturation-matric potential relations in gravel, *Water Resour. Res.*, *38*, 1214, doi:10.1029/2001WR001242.

Tokunaga, T. K., K. R. Olson, and J. Wan (2003), Moisture characteristics of Hanford gravels: Bulk, grain-surface, and intragranular components, *Vadose Zone J.*, *2*, 322–329.

Tokunaga, T. K., K. R. Olson, and J. Wan (2004), Conditions necessary for capillary hysteresis in porous media: Tests of grain size and surface tension influences, *Water Resour. Res.*, *40*, WO5111, doi:10.1029/2003WR002908.

Tripp, C. P., and J. R. Combes (1998), Chemical modification of metal oxide surfaces in supercritical CO_2: The interaction of supercritical CO_2 with the adsorbed water layer and the surface hydroxyl groups of a silica surface, *Langmuir*, *14*(26), 7350–7352.

Valvatne, P. H., and M. J. Blunt (2004), Predictive pore-scale modeling of two-phase flow in mixed wet media, *Water Resour. Res.*, *40*, W07406, doi:10.1029/2003WR002627.

van Genuchten, M. T. (1980), A closed-form equation for predicting the hydraulic conductivity of unsaturated soils, *Soil Sci. Soc. Am. J.*, *44*, 892–898.

Wang, S., I. M. Edwards, and A. F. Clarens (2013), Wettability phenomena at the CO_2-brine-mineral interface: Implications for geologic carbon sequestration, *Environ. Sci. Technol.*, *47*(1), 234–241.

Weast, R. C. (Ed.) (1977), *CRC Handbook of Chemistry and Physics*, 58 ed., F-43 pp., CRC Press, Cleveland, Ohio.

Zhou, Q. L., J. T. Birkholzer, E. Mehnert, Y. F. Lin, and K. Zhang (2010), Modeling basin- and plume-scale processes of CO_2 storage for full-scale deployment, *Ground Water*, *48*(4), 494–514.